 CMC, vol.42, no.2, pp.103-124, 2014

Design, Fabrication, Characterization and Simulation of PIP-SiC/SiC Composites

S. Zhao[1], Zichun Yang[1,2], X.G. Zhou[3], X.Z. Ling[4], L.S. Mora[5], D. Khoshkhou[6] and J. Marrow[5]

Abstract Continuous SiC fiber reinforced SiC matrix composites (SiC/SiC) have been studied and developed for high temperature and fusion applications. Polymer impregnation and pyrolysis (PIP) is a conventional technique for fabricating SiC/SiC composites. In this research, KD-1 SiC fibers were employed as reinforcements, a series of coatings such as pyrocarbon (PyC), SiC and carbon nanotubes (CNTs) were synthesized as interphases, PCS and LPVCS were used as precursors and SiC/SiC composites were prepared via the PIP method. The mechanical properties of the SiC/SiC composites were characterized. Relationship between the interphase shear strength and the fracture toughness of the composites was established. X-ray tomographic scans of the SiC/SiC composites were performed and the closed porosities of the composites were calculated. The compatibility of the SiC/SiC composites with liquid LiPb at 800 ˚C and 1000 ˚C was investigated. High-resolution synchrotron X-ray tomography was applied to the SiC/SiC composite and digital volume correlation was employed for Hertzian indentation testing of the SiC/SiC composite. A Cellular Automata integrated with Finite Elements (CAFE) method was developed to account for the effect of microstructure on the fracture behavior of the SiC/SiC composite.

Keywords: SiC/SiC composites, Microstructure, Properties, Simulation.

[1] Laboratory of Marine High-temperature Structural Composites, Naval University of Engineering, Wuhan, China.

[2] Corresponding author. Address: College of Power Engineering, Naval University of Engineering, Jiefang Ave. 717, Wuhan 430033, China. Tel.: +86-27-83635194; fax: +86-27-83638709. E-mail: yangzichun11@sina.com

[3] Science and Technology on Advanced Ceramic Fibers and Composites Laboratory, National University of Defense Technology, Changsha, China.

[4] Institute of Plasma Physics, Chinese Academy of Sciences, Hefei, China.

[5] Department of Materials, University of Oxford, Oxford, UK.

[6] Department of Metallurgy and Materials, University of Birmingham, Birmingham, UK.

1 Introduction

Silicon carbide (SiC) has been considered as a promising material for high temperature applications including gas turbines and aerospace propulsion systems [Naslain (2004)], nuclear reactors [Katoh, Snead, Henager Jr, Hasegawa, Kohyama, Riccardi and Hegeman (2007)], high temperature semiconducting devices [Powell and Rowland (2002)], membranes [Lee and Tsai (2000)] and catalyst carriers [Nguyen and Pham (2011)] owing to its attractive properties such as high Young's modulus and hardness, excellent thermal and chemical stability [Madar (2004)]. Consolidated SiC ceramics are usually prepared by various sintering techniques [Lomello, Bonnefont, Leconte, Herlin-Boime and Fantozzi (2012)] and polymer deriving methods [Novak and Iveković (2012)].

To overcome the brittle nature of SiC, continuous SiC fiber reinforced SiC matrix composites (SiC/SiC) are designed to have a pseudo-ductile and predictable fracture mode and tailorable physical and mechanical properties while taking advantage of most of the inherent merits of monolithic SiC [Snead, Nozawa, Ferraris, Katoh, Shinavski and Sawan (2011)]. SiC/SiC composites exhibit superior characteristics such as high operating temperature, chemical stability and low radio-activation [Iveković, Novak, Dražić, Blagoeva and Vicente (2013)].

The SiC/SiC composites are fabricated by various methods such as chemical vapor infiltration (CVI), nano infiltration and transient eutectic (NITE) and polymer impregnation and pyrolysis (PIP), et al. Among the alternative fabrication processes, PIP method is based on the principle of filling the porosity inside the fiber preforms with a SiC matrix resulting from decomposition of pre-ceramic polymer precursors [Shimoda, Park, Hinoki and Kohyama (2008)]. It offers advantages in the viewpoint of large-scale components fabrication with complex shapes, microstructural control, and low fabrication cost [Zhao, Zhou, Yu and Mummery (2013)].

However, the disadvantages of PIP lie in the low density, low purity and amorphous structure of the resultant matrix, it has been suggested that enhanced matrix crystallization and improved stoichiometry could be attained by elevating the pyrolysis temperature and novel polymer precursors [Nozawa, Hinoki, Hasegawa, Kohyama, Katoh, Snead, Henager and Hegeman (2009)]. PIP-SiC/SiC composites pyrolyzed at 1750∼1800 ˚C were fabricated by Y. Katoh et al. [Katoh, Kotani, Kishimoto, Yang and Kohyama (2001)], and their outstanding radiation stability was demonstrated. C. Nannetti et al. [Nannetti, Ortona, Pinto and Riccardi (2004)] prepared PIP-SiC/SiC composites with a final high-temperature pyrolysis treatment at 1700 ˚C, after which the thermal diffusivity of the composites increased noticeably. Moreover, near-stoichiometric SiC matrix was developed by blending of polycarbosilane (PCS) and polymethylsilane (PMS) [Kohyama, Kotani, Katoh,

Nakayasu, Sato, Yamamura and Okamura (2000)]. And allylhydridopolycarbosilane (AHPCS) is able to be converted in stoichiometric crystalline SiC, making the PIP process quite attractive [Kotani, Katoh, Kohyama and Narisawa (2003)].

In this work, SiC/SiC composites with various fiber textures, interphases and precursors were fabricated by PIP method, the microstructures of the SiC/SiC composites were investigated, the properties including mechanical properties, thermal conductivity and compatibility with LiPb were characterized. A Cellular Automata Finite Elements (CAFE) method was developed to account for the effect of microstructure on the fracture behavior of the SiC/SiC composite.

2 Materials

2.1 Reinforcement and architectures

KD-I SiC fiber bundles (provided by National University of Defense Technology, NUDT, China) were used as the reinforcement. KD-I is a Generation I SiC fiber consisted of crystalline β-SiC, amorphous Si-C-O and free carbon phase, general characteristics of the fiber are shown in Table 1 [Wang, Mao, Song and Wang (2009)].

Table 1: Typical characteristics of the KD-I SiC fiber.

Trademark	KD-I
Diameter (μm)	13.3
Density (g/cm^3)	2.45
Tensile strength (GPa)	1.8-2.2
Elastic modulus (GPa)	150-200
$\beta-$SiC content (%)	10
Oxygen content (wt%)	18.9

Uni-directional (UD), 2D, 2.5D and 3D (3-dimensional 4-directional [Yang, Cui, Nie, Wu, Yang and Wu (2013)]) preforms were fabricated using KD-I fibers in this work, the architectures of the fabrics are shown in Fig. 1.

2.2 Interphases

The importance of fiber-matrix interphase on mechanical properties of ceramic matrix composites (CMCs) has long been recognized. The major functions of an interphase are to prevent fibers from being corroded, transfer load between the fiber

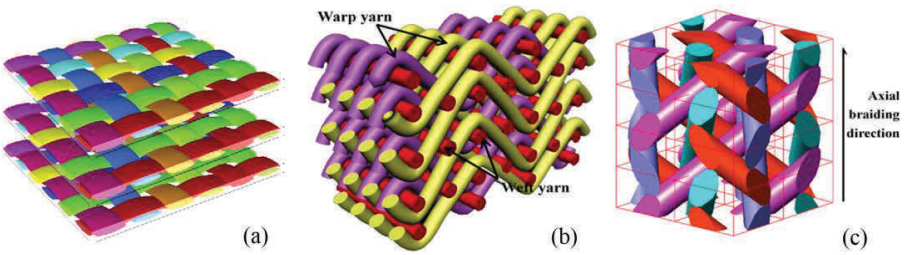

Figure 1: Architectures of (a) 2D, (b) 2.5D and (c) 3D4d fabrics.

and matrix, and arrest or deflect the cracks propagation in the matrix [Xiang, Li, Wang and Chen (2012)].

In this work, monolayer PyC, SiC, multilayer PyC/SiC and carbon nanotubes (CNTs) interphases were synthesized by chemical vapor deposition (CVD) process. Mixtures of methane and hydrogen gases were used to deposit PyC at 1100 ˚C, mixtures of methyltrichlorosilane (MTS), argon and hydrogen were used to deposit SiC at 1200 ˚C and mixtures of hydrogen, ethyne and nitrogen gases were used to grow CNTs at 750 ˚C. Typical appearances of the interphases are shown in Fig. 2.

Pyrocarbon (PyC) is the most commonly used interphase material in SiC/SiC composites for its superior functions in control of the crack defection at the interphase and load transfer between matrix and reinforcement. However, carbon is not stable under oxidizing or neutron irradiation conditions at high temperatures. Therefore, (PyC/SiC)n multilayer interphases are designed and developed. A multilayered interphase composed of a sequence of very thin PyC and SiC has several advantages, it is more resistant to oxidation and irradiation, it promotes multiple crack deflections between layers and enhances fiber/matrix interfacial shear strength, resulting in improved toughness of the composites [Bertrand, Droillard, Pailler, Bourrat and Naslain (2000)].

Carbon nanotubes (CNTs) are considered as promising nano-reinforcement applied in composites for their excellent mechanical and thermal properties [Yu, Zhou, Zhang, Peng, Zhang and Sun (2011)]. CVD and electrophoretic deposition (EPD) processes have been employed for preparing CNT interface layer on the SiC fibers [Sun, Yu, Zhang and Zhou (2011)].

The typical thickness of PyC interphase ranged between ∼20 nm (for the case of the sublayers in the multilayer interphase) and ∼500 nm, the typical thickness of SiC interphase ranged between ∼20 nm and ∼700 nm. The CNTs were several microns in length, randomly oriented with curved morphology, and homogeneous both at the surface and in the interior of the preform.

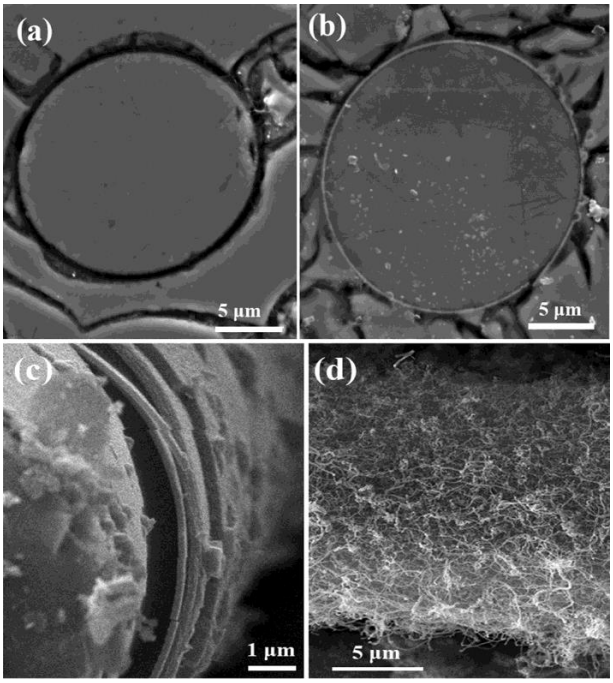

Figure 2: Micrographics of (a) PyC, (b) SiC (c) (PyC/SiC)n and (d) CNTs interphases.

2.3 Precursors

PIP method is based on the common principle of filling the porosity inside the fiber fabrics with a SiC matrix resulting from decomposition of pre-ceramic polymer precursors [Chen, Hu, Zhang, He and Mei (2011)]. In this work, two types of polymer precursors were used: the conventional, commonly used polycarbosilane (PCS) and the newly invented LPVCS. LPVCS is a mixture of V4 (2,4,6,8-tetravinyl-2,4,6,8-tetramethylcyclotetrasiloxane) and LPCS (low molecular weight PCS). The structural formulas of the precursors are shown in Fig. 3.

Characteristics of the precursors are shown in Table 2, the liquid precursor LPVCS has a low viscosity, a good stability and an excellent wetting property against SiC fiber. The ceramic yields of PCS and LPVCS are 65.1 % and 59.5 %, however, PCS should be dissolved in xylene before impregnation, so the ceramic yield of LPVCS is actually much higher.

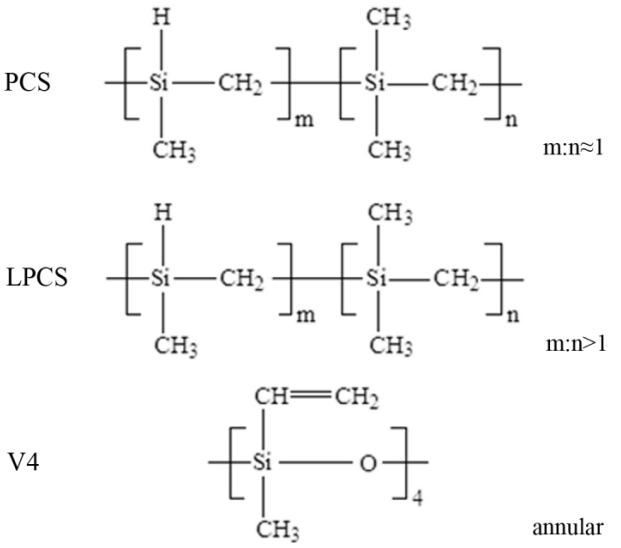

Figure 3: Structural formulas of the precursors

Table 2: Characteristics of the precursors.

Precursor	PCS	LPVCS
State at RT	solid	liquid
Viscosity (mPa•s)	25.0 (dissolved in xylene)	20.0
Stability	good	good (protected from light)
Ceramic yield (%)	65.1	59.5

3 Experimental methods

3.1 Fabrication of the SiC/SiC composites

The fabrication process of the SiC/SiC composites is shown in Fig. 4.

SiC/SiC composites were fabricated by PIP method in the following procedures composed of five steps.

(1) Fabrication of fiber preforms. SiC fiber bundles were woven or braided into preforms with various textures (UD, 2D, 2.5D and 3D).

(2) Fabrication of fiber coating. The preforms were in-situ deposited with PyC, SiC, (PyC/SiC)n or CNTs as the interphases.

(3) Impregnation of precursors. The coated preforms were impregnated with PCS

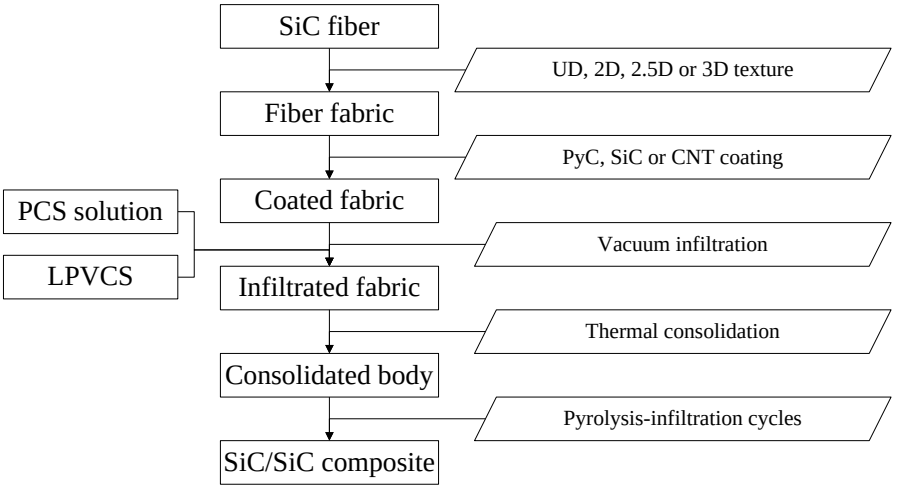

Figure 4: Fabrication process of PIP-SiC/SiC composites.

solution or LPVCS by a vacuum infiltration method.

(4) Consolidation process. The preforms were stacked into a special mould and heated up to the softening point of PCS (180 ˚C) or the crosslink temperature of LPVCS (300 ˚C), where a pressure-assisted consolidation process was applied with a certain uni-directional pressure.

(5) Pyrolysis-infiltration cycles. The consolidated bodies were pyrolyzed at 1100∼ 1200 ˚C in an inert Argon atmosphere. Then the impregnation and pyrolysis processes were repeated without pressurization until weight increase of the composites was less than 1%.

3.2 Methods of property evaluations

The bulk density and open porosity of the composites were determined by Archimedes' principle. Closed porosity was investigated by X-ray tomographic technique, the specimens were scanned using a Metris X-tek 320 kV source at the Henry Moseley X-ray Imaging Facility, University of Manchester, UK. The X-ray source voltage and current were set at 75 kV and 65 μA, respectively. The exposure time was 4000 ms per radiograph. CT-Pro software was used for tomographic reconstruction and Avizo 6 Standard software was used for 3D visualization.

Bending strength and modulus of the composites were characterized by three-point bending tests following GBT 6569-2006, with the specimen size of 4 mm $\times$ 4 mm $\times$ 65 mm, the crosshead speed of 0.5 mm/min and outer support span of 50

mm. Fracture toughness was tested by simple edge notch beam (SENB) method following GBT 23806-2009, with the specimen size of 4 mm $\times$ 8 mm $\times$ 65 mm, the notch length 4 mm, the crosshead speed of 0.05 mm/min and outer support span of 40 mm. 5 specimens were tested for the tests.

Interfacial shear property was obtained by the single fiber push-out test. Isolated fibers were selected using a video microscope and were pushed out using a Berkovich-type pyramidal diamond indenter tip. Interfacial shear properties were obtained by the single fiber push-out test. Samples were sliced from composite specimens normal to the fiber direction into 1 mm-thick sections, which were mechanically polished to a final thickness of approximately 100 μm. During the test, specimens were mounted on top of a holder containing a groove of 40 μm wide. Isolated fibers with the fiber direction perpendicular to the holder surface on the groove were selected using a video microscope and were pushed out using a Berkovich-type pyramidal diamond indenter tip with the maximum load ability of 1 N.

Thermal diffusivity was measured in the through-thickness direction at ambient temperature using a laser-flash method according to GB 11108-89. Specific heat was measured according to GBT 10295-2008 using the same specimens.

Corrosion tests of the SiC/SiC composites were performed at 800 ˚C for 200 h and 1000 h, and at 1000 ˚C for 200 h in isothermal conditions in a high-purity argon atmosphere. The specimens were placed in different Mo crucibles with lids, and all the crucibles were filled with liquid LiPb and set in a glove box.

The high-resolution synchrotron X-ray computed tomography was performed at the Diamond Light Source, beamline I12, using radiographic projections obtained at an X-ray beam energy of 53 keV. Each radiograph had an acquisition time of 2 seconds with projections at increments of 0.03 degrees over 180˚ rotation. The specimen, a rectangular prism (3 $\times$ 3 mm square, 3 mm high), was indented by a 5 mm radius Al_2O_3 ball under displacement control using a Hertzian indentation loading stage.

Morphology and structure of the specimens were analyzed by scanning electron microscopy (SEM), X-Ray Diffraction (XRD) and transmission electron microscopy (TEM) equipped with a selected-area electron diffraction (SAED) unit.

4 Results and discussion

4.1 Microstructure

Detailed microstructures of the PIP-SiC/SiC composites varied substantially, depending on the processing conditions. Typical microstructures of a (PyC/SiC)n multilayered SiC/SiC composite observed by TEM are shown in Fig. 5. KD-I

SiC fiber was mostly amorphous with a small amount of microcrystalline β-SiC and residual carbon (Fig. 5b). PyC interphase exhibited a fairly high-density turbostratic graphite structure, CVD SiC interphase was pure, crystalline and near stoichiometric β-SiC (Fig. 5c). PCS derived SiC matrix consisted of crystalline β-SiC, amorphous Si-C-O and free carbon phase (Fig. 5d).

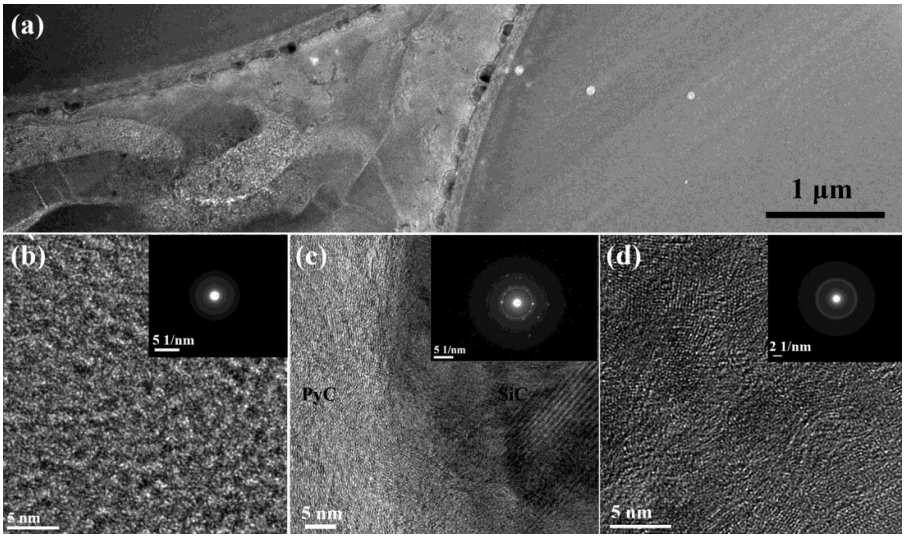

Figure 5: TEM images of SiC/SiC composite with (PyC/SiC)n multilayer (a) Higher magnification micrographs are given for (b) the fiber, (c) interphase, and (d) matrix.

TEM images of the CNTs and LPVCS derived SiC matrix are shown in Fig. 6. The CNTs synthesized by CVD method are clean and catalyst nanoparticles can be seen clearly at the CNT tips (Fig. 6a), which indicates the vapor-liquid-solid (VLS) growth mechanism of the CNTs. Inset of Fig. 6a shows an HRTEM image of the CNT, which reveals the atomic structure of the as-grown CNTs and the multiwalled structure is confirmed. As shown in Fig. 6b, SiC matrix derived from LPVCS at 1100 ˚C is completely amorphous, which is demonstrated by the SAED pattern (Fig. 6b, insert).

4.2 Density and porosity

The densities and open porosities of the SiC/SiC composites are shown in Table 3. The densities of the composites ranged from 1.97$\sim$2.34 g·cm^{-3}, depending on the different fiber textures and volume fractions. The low densities were determined

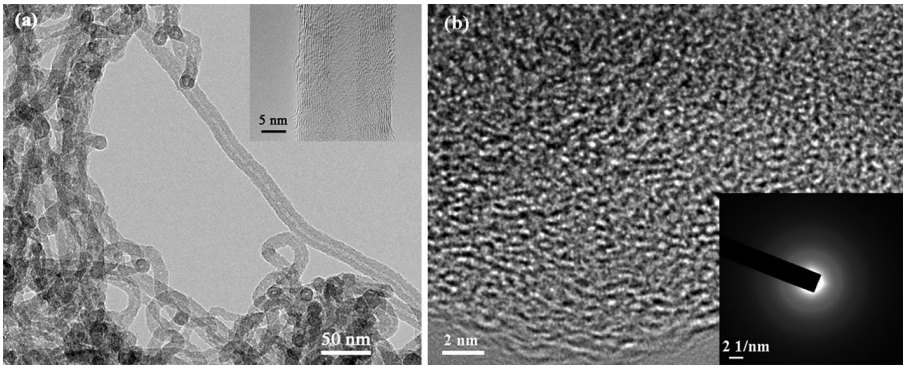

Figure 6: TEM images of (a) CNTs and (b) LPVCS derived matrix.

by the porous, amorphous and non-stoichiometry nature of the PIP-SiC/SiC composites. The open porosity of the SiC/SiC composite fabricated with LPVCS was 2.9 %, much lower than those fabricated with PCS, indicating a high densification efficiency of the LPVCS.

Table 3: Properties of the SiC/SiC composites.

Texture	1D	2D	2.5D	3D-4d				
Fiber volume fraction (%)	-	27.2	43	~ 40				
Interphase	SiC				PyC	(PyC/SiC)n	CNTs	PyC
Precursor	PCS							LPVCS
Density (g/cm^3)	2.34	2.09	2.13	2.17	2.18	2.24	1.97	2.17
Open porosity (%)	7.5	11.1	8.1	8.8	7.4	6.4	10.5	2.9
Thermal conductivity (W/m·K)	-	0.85	1.14	1.24	1.26	1.20∼1.56	1.83	1.64
Bending strength (MPa)	701.1	363.3	306.5	353.0	576.7	334.7	354.5	657.9
Fracture toughness (MPa·m$^{1/2}$)	26.6	7.8	9.6	12.18	25.7	28.1	23.2	29.5

Closed porosities of the 2.5D and 3D SiC/SiC composites were investigated by X-ray tomographic techniques. Shape, distribution and volume of the pores could be observed or calculated after 3D visualization of the composites (shown in Fig. 7). The voxel size of the 3D volume is approximately 5.3μm due to the distance

between source, sample and detector, so only macropores with size $>5.3\mu$m could be distinguished.

The closed porosity of 2.5D SiC/SiC composite was only 3.1%, indicating most of the pores in 2.5D composites were open pores. The closed porosity of 3D SiC/SiC composite fabricated with PCS was 9.2%, which was quite close to its open porosity. 3D SiC/SiC composite fabricated with LPVCS proved to be much less porous, with a closed porosity of 4.6 %.

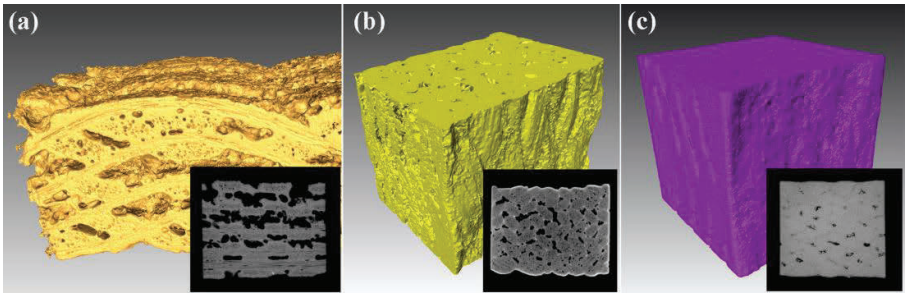

Figure 7: 3D images of the SiC/SiC composites, (a) 2.5D composite, (b) 3D composite fabricated with PCS and (C) 3D composite fabricated with LPVCS, the inserts are the reconstructed cross-section images.

4.3 Mechanical properties

SiC/SiC composites reinforced with 2.5D and 3D braided fiber fabrics are developed because their delaminating resistance and thermal conductivity in z-direction superior to that of the conventional laminated composites [Nannetti, Riccardi, Ortona, Barbera, Scafè and Vekinis (2002)]. Mechanical properties of the SiC/SiC composites are shown in Table 3. The bending strength and fracture toughness of 3D SiC/SiC composite with PyC interphase were 576.7 MPa and 25.7 MPa·m$^{1/2}$, which were much higher than those of the 3D SiC/SiC composite with SiC interphase, indicating that the PyC was a suitable interphase for SiC/SiC composites.

A series of (PyC/SiC)n multilayer coatings were deposited onto SiC fibers. Cracks were found to deflect and branch between interphases and fibers, between different sublayers, and/or inside a PyC sublayer, where a large amount of fracture energy was consumed. However, the propagation of the main matrix crack was still within the first PyC sublayer (Fig. 8).

Single-fiber push-out tests were carried out to evaluate the shear strength of various fiber-matrix interphases (shown in Fig. 9). Using the as-received KD-I SiC fiber

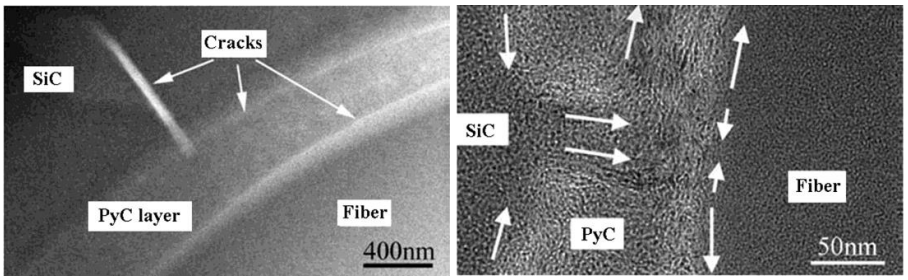

Figure 8: Propagation of the cracks at the interphases, (a)PyC and (b) (PyC/SiC)n.

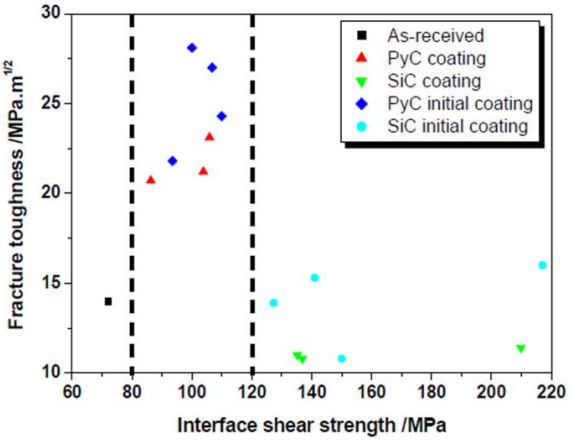

Figure 9: Relationship between the interphase shear strength and the fracture toughness of the SiC/SiC composites.

yielded a weak interfacial bond between the fiber and matrix (72.1 MPa). This together with the inevitable corrosion to the fiber during the manufacturing process led to a relatively weak composite. The interphase shear strength of the composites increased to a maximum of 105.9 MPa for the PyC coating. Reinforcing with the CVD SiC coated KD-I fiber resulted in a very strong interphase, the highest interphase shear strength of the SiC coating was 209.8 MPa. A range between 93.5 MPa and 150.0 MPa was found for the PyC initial coatings. The composites reinforced with PyC-coated and PyC initial coated KD-I fibers exhibited much improved mechanical properties compared to the composites containing the as-received, SiC coated and SiC initial coated fibers, indicating that an appropriate strengthening to the interphase bonding was expected to improve the fracture toughness of the composites [Yu, Zhou, Zhang, Peng, Zhang and Huang (2011)].

The bending strength and fracture toughness of the SiC/SiC composite fabricated with LPVCS were 657.9 MPa and 29.5 MPa·$m^{1/2}$. The improvement of the mechanical properties could be attributed to the lower porosity of the LPVCS derived matrix with fewer microcracks.

4.4 Thermal conductivity

The thermal conductivity of the SiC/SiC composite is calculated according to the formula below:

$$\lambda = 418.68 \times \alpha \times Cp \times \rho \tag{1}$$

Where λ is the thermal conductivity (W/m·K), α is the thermal diffusivity (cm^2/s), Cp is the specific heat (cal/g·K) and ρ is the density (g/cm^3).

As shown in Table 3, the thermal conductivities of the PIP-SiC/SiC composites are low (<2 W/m·K). The KD-I SiC fiber and PCS derived SiC matrix were mostly amorphous with a small amount of microcrystalline β-SiC and residual carbon, LPVCS derived SiC matrix was completely amorphous, all exhibiting intrinsic low thermal conductivities. Moreover, the pores in the composites contained nonconductive gas and caused the scattering of phonon, while the interphases, microcracks and defects acted as thermal barriers [Yang, Su and Sun (2013)]. All above led to the low transverse thermal conductivities of the SiC/SiC composites. 3D composites had higher portion of fiber bundles in z-direction, resulting in higher thermal conductivity than 2D and 2.5D composites. SiC/SiC composite with CNTs interphase exhibited the highest thermal conductivity because CNTs are highly conductive [Akbarov (2013)]. However, the CNTs were agglomerated and no conducting network was formed (Fig. 10), hence the thermal conductivity of the CNTs-SiC/SiC composite was still insufficient.

4.5 Compatibility with liquid LiPb

After exposure to liquid LiPb at 800 ˚C for 200 h, the surface morphology of the SiC/SiC composite changed slightly (Fig. 11a and 11b). So we extended the exposure duration to 1000 h, after which the surface of the SiC/SiC composite became rough (Fig. 11c), indicating that SiC is dissolved in the liquid LiPb. The XRD analysis of the composite showed no obvious phase changes after 1000 h exposure (Fig. 12).

In order to identify the reaction product, corrosion test at 1000 ˚C for 200 h was carried out. Significant changes were observed after the test, a lot of pores and cracks were seen on the roughened surface (Fig. 11d). Moreover, β-SiC peaks disappeared and two new phases, $Al_{0.7}Fe_3Si_{0.3}$ and $Cr_{37}Nb_{27}Si_{36}$ were detected

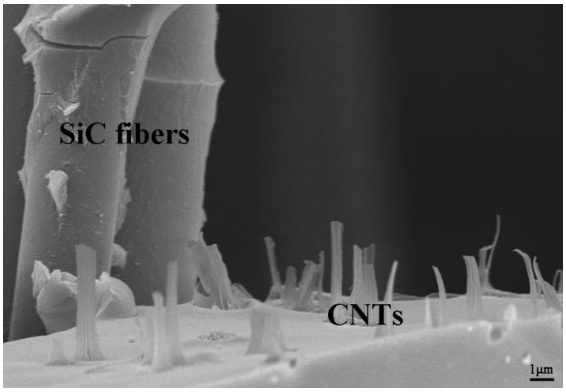

Figure 10: Morphology of the agglomerated CNTs in the SiC/SiC composites

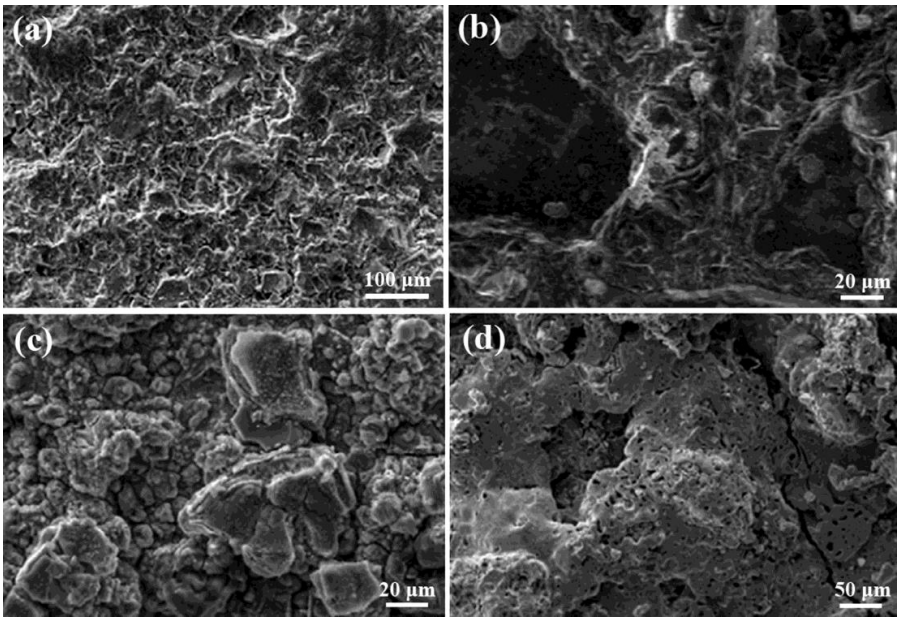

Figure 11: Surface morphologies of the SiC/SiC composite before and after exposure to liquid LiPb, (a) as-received, (b) after 200 h at 800˚C, (c) after 1000 h at 800˚C and (d) after 200 h at 1000˚C.

from the XRD pattern after corrosion (Fig. 12), indicating that SiC reacted with metal impurities in the liquid LiPb. The impurities resulted from the dissolution of alloy lids into the liquid LiPb, which is quite similar to the previous report where

SiC reacted with Ni impurity in the LiPb [Zhao, Zhou, Yu, Wang, Wu, Huang, Zhu and Huang (2010)].

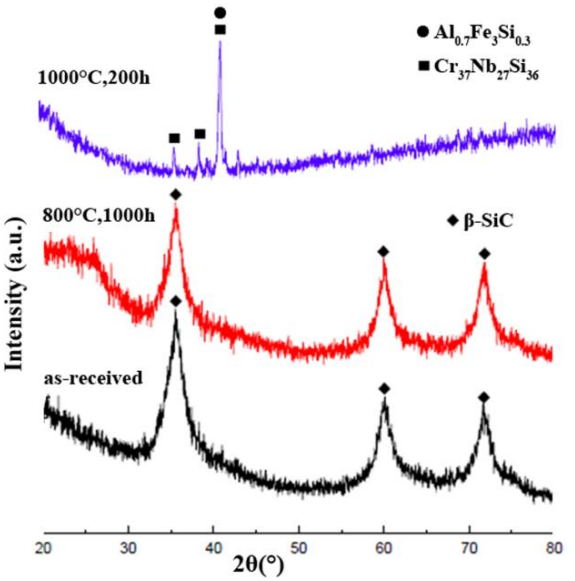

Figure 12: XRD patterns of the SiC/SiC composite before and after corrosion tests.

4.6 Modeling and experimental observation of damage

High-resolution synchrotron X-ray tomography was performed on the 3D PCS-SiC/SiC composite. The nominal voxel size was 0.9 μm. Vertical slices through the tomography data are shown in Fig. 13.

The complexity of the microstructure was clear. Large macropores, fine micropores and oriented bundles of fibers with elongated inter-fiber pores were observed. The damage induced by the indentation occurred over a length scale that was comparable to the lengthscale of the microstructure [Mora, Mostafavi, Khoshkhou, Reinhard, Atwood, Zhao, Connolly and Marrow (2013)].

The tomographic data of the scanned specimen were analyzed using the Avizo Fire software to obtain a statistical description of the porosity, which was used subsequently to create the CAFE (cellular automata integrated with finite element) simulation [Mora and Marrow (2013)]. To establish the CAFE model, the main significant microstructure features that were observed experimentally, which were the inter-fiber pores and also the significant macro pores were reproduced numerically. The elongated inter-fiber pores were distributed randomly in the simulation

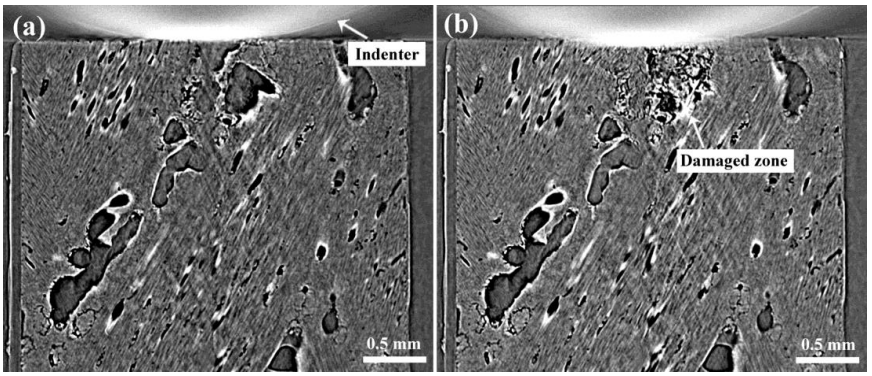

Figure 13: Vertical slice through the tomographic image of the SiC/SiC composite, (a) before indentation and (b) in situ under indentation.

of the specimen within the identified bounds of the fiber bundles, with their dimensions, orientation and position defined randomly using parameters from their measured statistical distributions (Fig. 14). The macro and micropores were similarly distributed randomly in the matrix. The model therefore consisted of SiC matrix and SiC fibers within the fiber bundles with mechanical properties given in Table 4 [Zhao, Zhou, Yu and Mummery (2013)], and empty pores. The mechanical properties of the matrix and the fibers were obtained by nano-indentation method [Pulla and Lu (2012)]. The cells around the inter-fiber pores were assigned the matrix modulus but with a lower strength in order to be able to simulate a weaker interfacial strength between fibers.

Table 4: Properties of the SiC/SiC composites.

3D PCS-SiC/SiC composite	Fiber	Matrix
Modulus(GPa)	115.06	187.65
Hardness(GPa)	14.12	20.03

The DVC analyses were carried out using the Davis StrainMaster 8.1 software, correlating the loaded 3D tomographic dataset against the unloaded reference to map the relative displacements (Fig. 15a). The CAFE simulation predicted a similar sized zone of high strain, with some local strain concentrations due to the macropores (Fig. 15b). The slight asymmetry in the experimental data might be due to either to anisotropy of the microstructure or a component of shear loading from misalignment of the loading rig.

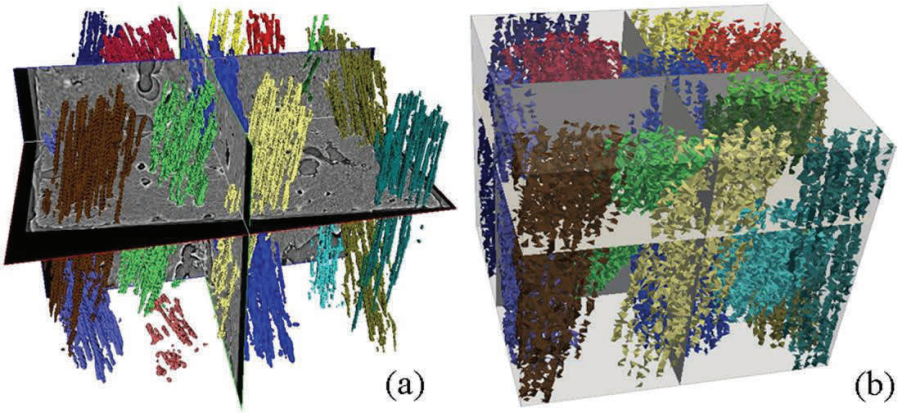

Figure 14: Inter-fiber pore distributions within fiber groups, (a) experimentally observed structure after segmentation, (b) numerical simulation.

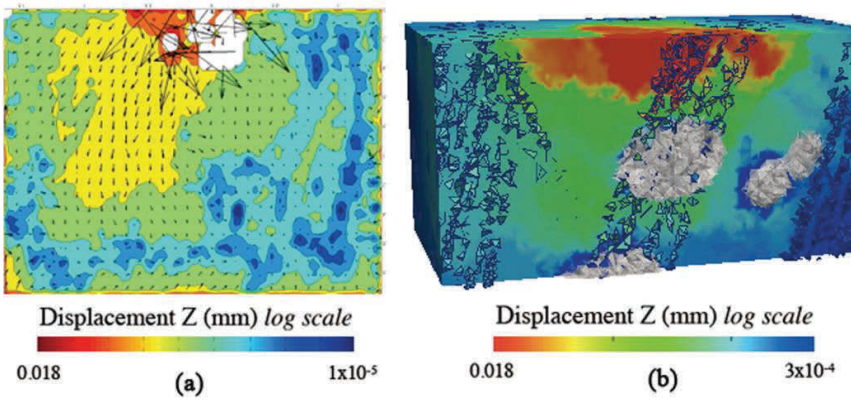

Figure 15: Comparison between experiment and CAFE simulation in a vertical section (3 mm $\times$ 2 mm) under the indentation, (a) Experimental data with displacement vectors overlaid (white areas have poor correlation) and (b) CAFE simulation of displacements showing inter-fibre pores and macro-pores.

Further comparison is made using the compressive displacements along the z-axis under the indentation (i.e. at x=1.5 mm and y=1.5 mm), which is shown in Fig. 16 together with quarter slices of the CAFE numerical simulation in which the macro-pores are shown and a Finite Element Modeling (FEM) simulation (ABAQUS) using the same damage model. As the CAFE simulation cells are not necessarily

located exactly on the z-axis, the displacement data for all the cells within 1/30 of the side length (i.e. 100 μm) from the z-axis are shown. For the strain data in Fig. 16c, due to the variations in the CAFE displacements, only representative strain values from cells on the z-axis are plotted. The agreement between the experiment, CAFE simulation and FEM-damage simulation is generally good, particularly remote from the indentation where the deformation is elastic. The data for a simple elastic FEM simulation are also shown; agreement is good only in the elastic region. The variability in the CAFE displacements is due to the local effects of pores on the development of damage; there is a significant influence from the large pore that is beneath the indentation, which is generally consistent with the observed effect of a similar sized pore in the experimental data. The FEM simulation with damage does not capture this behavior.

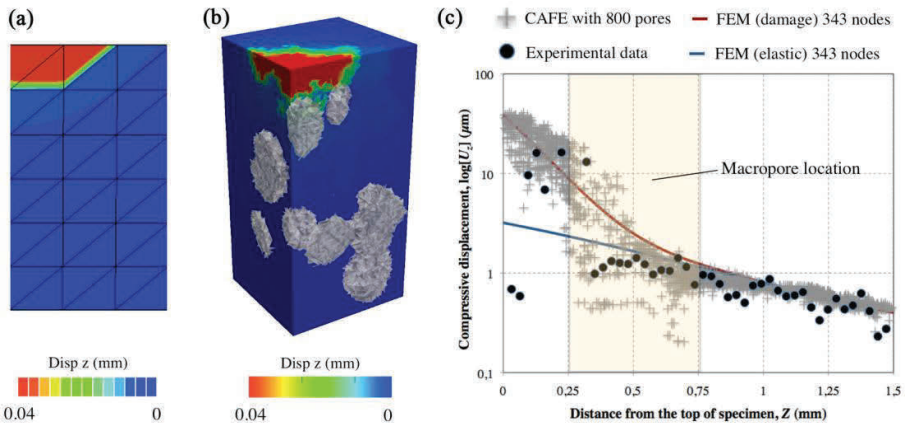

Figure 16: Comparison between the numerical and experimental vertical compressive displacement, (a) FEM simulation with damage, (b) CAFE simulation and (c) displacements along z-axis.

5 Conclusions

SiC/SiC composites were fabricated by PIP method using KD-1 SiC fibers as reinforcements, a series of coatings such as PyC, SiC, (PyC/SiC)n and CNTs as interphases, and PCS and LPVCS as precursors.

SiC/SiC composites fabricated with PyC interphase and LPVCS as the precursor exhibited superior flexural strength and fracture toughness.

The interphase shear strength of the composites were evaluated, the results indicated that an appropriate strengthening to the interphase bonding was expected to

improve the fracture toughness of the composites.

The compatibility of the SiC/SiC composites with LiPb at 800 ˚C and 1000 ˚C was investigated. Corrosion was caused by reaction between SiC and metal impurities in the liquid LiPb.

High-resolution synchrotron X-ray tomography was applied to the 3D PCS-SiC/SiC composite. DVC was employed for Hertzian indentation testing of the SiC/SiC composite, quantifying damage by measurement of the displacement fields within the material. A CAFE method was developed to account for the effect of microstructure on the fracture behavior of the SiC/SiC composite. Graded microstructures, textures and multiple phases were simulated and a mesh-free framework was developed to compute the damage development through the microstructure. The results demonstrated the applicability of the modeling strategy to damage development, parallelization of the CAFE computations will increase the efficiency compared to FEM simulations of similar fidelity and discretisation.

Acknowledgement: The authors are grateful for the financial support from Aid program for Science and Technology Innovative Research Team in Higher Educational Institutions of Hunan Province and Aid program for Innovative Group of National University of Defense Technology. The Modeling work was carried out with the support of the UK EPSRC project "QUBE: Quasi-Brittle fracture: a 3D Experimentally-validated approach" (EP/J019992/1). The authors acknowledge the beam time award at the Joint Engineering, Environmental and Processing (I12) beamline (Experiment EE7730).

References

Akbarov, S. D. (2013): On Axisymmetric Longitudinal Wave Propagation in Double-Walled Carbon Nanotubes. *CMC: Computers, Materials & Continua,* vol. 33, pp. 63-85.

Bertrand, S.; Droillard, C.; Pailler, R.; Bourrat, X.; Naslain, R. (2000): TEM structure of (PyC/SiC)n multilayered interphases in SiC/SiC composites. *Journal of the European Ceramic Society,* vol. 20, pp. 1-13.

Chen, S.; Hu, H.; Zhang, Y.; He, X.; Mei, M. (2011): Rapid densification of C/SiC composites by joint process of CLVD and PIP. *Materials Letters,* vol. 65, pp. 3137-3139.

Iveković, A.; Novak, S.; Dražić, G.; Blagoeva, D.; Vicente, S. (2013): Current status and prospects of SiCf/SiC for fusion structural applications. *Journal of European Ceramic Society,* vol. 33, pp. 1577-1589.

Katoh, Y.; Snead, L. L.; Henager Jr, C. H.; Hasegawa, A.; Kohyama, A.; Ric-

cardi, B.; Hegeman, H. (2007): Current status and critical issues for development of SiC composites for fusion applications. *Journal of Nuclear Materials,* vol. 367–370, Part A, pp. 659-671.

Katoh, Y.; Kotani, M.; Kishimoto, H.; Yang, W.; Kohyama, A. (2001): Properties and radiation effects in high-temperature pyrolyzed PIP-SiC/SiC. *Journal of Nuclear Materials,* vol. 289, pp. 42-47.

Kohyama, A.; Kotani, M.; Katoh, Y.; Nakayasu, T.; Sato, M.; Yamamura, T.; Okamura, K. (2000): High-performance SiC/SiC composites by improved PIP processing with new precursor polymers. *Journal of Nuclear Materials,* vol. 283-287, pp. 565-569.

Kotani, M.; Katoh, Y.; Kohyama, A.; Narisawa, M. (2003): Fabrication and Oxidation-Resistance Property of Allylhydridopolycarbosilane-Derived SiC/SiC Composites. *Journal of the Ceramic Society of Japan,* vol. 111, pp. 300-307.

Lee, L. L.; Tsai, D. S. (2000): Synthesis and Permeation Properties of Silicon-Carbon-Based Inorganic Membrane for Gas Separation. *Industrial & Engineering Chemistry Research,* vol. 40, pp. 612-616.

Lomello, F.; Bonnefont, G.; Leconte, Y.; Herlin-Boime, N.; Fantozzi, G. (2012): Processing of nano-SiC ceramics: Densification by SPS and mechanical characterization. *Journal of the European Ceramic Society,* vol. 32, pp. 633-641.

Madar, R. (2004): Silicon carbide in contention. *Nature,* vol. 430, pp. 974–975.

Mora, L. S.; Mostafavi, M.; Khoshkhou, D.; Reinhard, C.; Atwood, R.; Zhao, S.; Connolly, B.; Marrow, T. J. (2013): 3D cellular automata finite element (CAFE) modelling and experimental observation of damage in quasi-brittle nuclear materials: Indentation of a SiC-SiC$_{fibre}$ ceramic matrix composite. *Third International Workshop on Structural Materials for Innovative Nuclear Systems*, Idaho Falls, USA.

Mora, L. S.; Marrow, T. J. (2013): 3D cellular automata finite element method to model quasi-brittle fracture. *Twelfth International Conference on Engineerng Structural Integrity Assessment*, Manchester, UK.

Nannetti, C. A.; Ortona, A.; Pinto, D. A. d.; Riccardi, B. (2004): Manufacturing SiC-fiber-reinforced SiC matrix composites by improved CVI/slurry infiltration/polymer impregnation and pyrolysis. *Journal of American Ceramic Society,* vol. 87, pp. 1205-1209.

Nannetti, C. A.; Riccardi, B.; Ortona, A.; Barbera, A.; Scafè, E.; Vekinis, G. (2002): Development of 2D and 3D Hi-Nicalon fibres/SiC matrix composites manufactured by a combined CVI–PIP route. *Journal of Nuclear Materials,* vol. 307–311, Part 2, pp. 1196-1199.

Naslain, R. (2004): Design, preparation and properties of non-oxide CMCs for application in engines and nuclear reactors: an overview. *Composites Science and Technology,* vol. 64, pp. 155-170.

Nguyen, P.; Pham, C. (2011): Innovative porous SiC-based materials: From nanoscopic understandings to tunable carriers serving catalytic needs. *Applied Catalysis A: General,* vol. 391, pp. 443-454.

Novak, S.; Iveković, A. (2012): SiC–CNT Composite Prepared by Electrophoretic Codeposition and the Polymer Infiltration and Pyrolysis Process. *The Journal of Physical Chemistry B,* vol. 117, pp. 1680-1685.

Nozawa, T.; Hinoki, T.; Hasegawa, A.; Kohyama, A.; Katoh, Y.; Snead, L. L.; Henager, C. H.; Hegeman, J. B. J. (2009): Recent advances and issues in development of silicon carbide composites for fusion applications. *Journal of Nuclear Materials,* vol. 386-88, pp. 622-627.

Powell, A. R.; Rowland, L. B. (2002): SiC materials-progress, status, and potential roadblocks. *Proceedings of the IEEE,* vol. 90, pp. 942-955.

Pulla, S. S.; Lu, Y. C. (2012): Effective Interfacial Thickness in Dissimilar Materials through Nanoindentation. *CMC: Computers, Materials & Continua,* vol. 29, pp. 263-278.

Snead, L. L.; Nozawa, T.; Ferraris, M.; Katoh, Y.; Shinavski, R.; Sawan, M. (2011): Silicon carbide composites as fusion power reactor structural materials. *Journal of Nuclear Materials,* vol. 417, pp. 330-339.

Shimoda, K.; Park, J. S.; Hinoki, T.; Kohyama, A. (2008): Influence of pyrolytic carbon interface thickness on microstructure and mechanical properties of SiC/SiC composites by NITE process. *Composites Science and Technology,* vol. 68, pp. 98-105.

Sun, K.; Yu, J.; Zhang, C.; Zhou, X. (2011): In situ growth carbon nanotube reinforced SiCf/SiC composite. *Materials Letters,* vol. 66, pp. 92-95.

Wang, D.; Mao, X.; Song, Y.; Wang, Y. (2009): Preparation and Properties of SiC Fiber with a Stable Excess Carbon Layer on the Surface. *Journal of Inorganic Materials,* vol. 24, pp. 1209-1213.

Xiang, Y.; Li, W.; Wang, S.; Chen, Z. H. (2012): Oxidation behavior of oxidation protective coatings for PIP–C/SiC composites at 1500˚C. *Ceramics International,* vol. 38, pp. 9-13.

Yu, H.; Zhou, X.; Zhang, W.; Peng, H.; Zhang, C.; Sun, K. (2011): Properties of carbon nano-tubes–Cf/SiC composite by precursor infiltration and pyrolysis process. *Materials & Design,* vol. 32, pp. 3516–3520.

Yu, H. J.; Zhou, X. G.; Zhang, W.; Peng, H. X.; Zhang, C. R.; Huang, Z. L.

(2011): Mechanical properties of 3D KD-I SiCf/SiC composites with engineered fibre–matrix interfaces. *Composites Science and Technology,* vol. 71, pp. 699-704.

Yang, Z. C.; Su, G. H.; Sun, F. R. (2013): Theoretical Modeling of the Radiative Properties and Effective Thermal Conductivity of the Opacified Silica Aerogel. *CMC: Computers, Materials & Continua,* vol. 36, pp. 271-292.

Yang, Z.; Cui, J.; Nie, Y.; Wu, Y.; Yang, B.; Wu, B. (2013): Microstructural Modeling and Second-Order Two-Scale Computation for Mechanical Properties of 3D 4-Directional Braided Composites. *CMC: Computers, Materials & Continua,* vol. 38, pp. 175-194.

Zhao, S.; Zhou, X. G.; Yu, H. J.; Wang, H. L.; Wu, Y. C.; Huang, Q. Y.; Zhu, Z. Q.; Huang, Z. L. (2010): Compatibility of PIP SiCf/SiC with LiPb at 700 degrees C. *Fusion Engineering and Design,* vol. 85, pp. 1624-1626.

Zhao, S.; Zhou, X.; Yu, J.; Mummery, P. (2013): Effect of heat treatment on microstructure and mechanical properties of PIP-SiC/SiC composites. *Materials Science and Engineering A,* vol. 559, pp. 808–811.

Zhao, S.; Zhou, X.; Yu, J.; Mummery, P. (2013): Fabrication and characterization of 2.5D and 3D SiCf/SiC composites. *Fusion Engineering and Design,* vol. 88, pp. 2453– 2456.